Journal of Scientific Computing (2020) 84:24
https://doi.org/10.1007/s10915-020-01270-5

Asymptotic Analysis for Overlap in Waveform Relaxation Methods for RC Type Circuits

Martin J. Gander[1] · Pratik M. Kumbhar[1] · Albert E. Ruehli[2]

Received: 21 October 2019 / Revised: 8 May 2020 / Accepted: 22 June 2020

Abstract
Waveform relaxation (WR) methods are based on partitioning large circuits into sub-circuits which then are solved separately for multiple time steps in so called time windows, and an iteration is used to converge to the global circuit solution in each time window. Classical WR converges quite slowly, especially when long time windows are used. To overcome this issue, optimized WR (OWR) was introduced which is based on optimized transmission conditions that transfer information between the sub-circuits more efficiently than classical WR. We study here for the first time the influence of overlapping sub-circuits in both WR and OWR applied to RC circuits. We give a circuit interpretation of the new transmission conditions in OWR, and derive closed form asymptotic expressions for the circuit elements representing the optimization parameter in OWR. Our analysis shows that the parameter is quite different in the overlapping case, compared to the non-overlapping one. We then show numerically that our optimized choice performs well, also for cases not covered by our analysis. This paper provides a general methodology to derive optimized parameters and can be extended to other circuits or system of differential equations or space–time PDEs.

Keywords Optimized waveform relaxation · RC circuits · Asymptotic analysis

1 Introduction

Electric circuits play a crucial role in our everyday life: they can be found in computers, cell phones, chargers, but also in cars, watches, and more and more household appliances like stoves, fridges and so on. Before buildings these circuits, they are usually simulated using computer programs. Simulating circuits means developing a mathematical model to replicate

✉ Pratik M. Kumbhar
pratik.kumbhar@unige.ch

Martin J. Gander
martin.gander@unige.ch

Albert E. Ruehli
ruehlia@mst.edu

[1] Section of Mathematics, University of Geneva, 1211 Geneva, Switzerland

[2] EMC Laboratory, Missouri University of Science and Technology, Rolla, MO, USA

Published online: 16 July 2020

the behavior of the real circuit, and then solve this model numerically. These simulations help the circuit designers to test their ideas, and optimize circuit parameters to achieve the desired output. Simulations save a lot of time and cost when designing circuits, and one can minimize the risk of unwanted hazards. Further, the number of electronic devices is continuously increasing tremendously which in turn increases the need for new design tools and techniques. Circuit solvers like the many different SPICE (Simulation Program with Integrated Circuit Emphasis) variants are no exception. Not only new approaches are desired but the tools need to have an ever increasing capacity to solve larger problems.

The specific class of problems considered in this work is a subset. We consider a sub-class of circuits which are called RC circuits which are composed of resistors (R) and capacitors (C). Of course, the circuits will also include current and voltage sources. This circuit is also called RC filter since it is used to filter certain frequencies and let pass others. The most common are high pass filters and low pass filters. We study here the low pass RC filter circuit which is shown in Fig. 1. This circuit allows signals with frequencies lower than a certain cut off frequency to pass. Such circuits are often used in acoustics, optics and electronics and hence their study is of great importance. We formulate an effective mathematical model for its simulation using the well known and widely used MNA (Modified Nodal Analysis) [29], which resembles the finite element assembly procedure in numerical partial differential equations (PDEs) [14,28]. This leads to a large system of ordinary differential equations (ODEs) where the unknowns are voltages at the nodes [29]. It is computational costly to solve such systems especially if their size is in the order of millions. Also, since 2004, the CPU frequency has been stagnating around 3 GHz and there is little hope that in the near future there will be any improvement [12]. Due to the availability of large numbers of processors, we are left with the option of using parallel computing in order to increase simulation speed. Over the years, various numerical tools have been developed to solve PDEs and large systems of equations effectively using parallel computing. One such tool is Waveform Relaxation.

Waveform Relaxation (WR) was developed in 1982 by Lelarasmee, Ruehli and Sangiovanni-Vincentelli [35], for analyzing electric circuits, and WR methods are discussed in the monographs [6,42,44]. In WR, the circuit or the system of differential equations is decomposed into many sub-circuits or subsystems which are then solved independently over an entire time window using standard time integration techniques. After each solve, information is transferred between neighboring subsystems using transmission conditions and the process is repeated until convergence is reached. The classical WR algorithm converges slowly when large time windows are used. To overcome this issue, smart transmission conditions were introduced, which led to optimized waveform relaxation (OWR) since different parameters in the transmission conditions need to be optimized. The convergence analysis of the classical WR methods for RC circuits was carried out by Ruehli et al [40]. Further, studies of WR and OWR algorithms applied to small RC circuits can be found in [2,16], and for large RC circuits, see [3,23,33]. There are also analyses at the discrete level for OWR applied to RC circuits [45]. WR and OWR were also studied for RLCG transmission lines

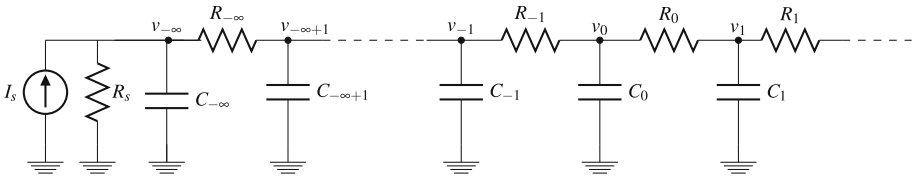

Fig. 1 RC circuit of infinite length

[1,15,20,21,25]. A different approach for the interconnect circuits has been studied in [36], where the interconnect circuit is partitioned using Norton interfaces which depend upon resistors. However, in all these references, both WR and OWR were studied for the case of non-overlapping circuits. We show here that WR for circuits is related to domain decomposition for PDEs, in the case of the RC circuit the heat equation [13,17], and for RLCG circuits the wave equation [19], and domain decomposition methods often use overlap to improve convergence. Overlap in WR methods for sparse linear differential systems was also tested early on in [7,32], and motivated the first WR methods for PDEs [17]. In this article, we study the effect of overlap on the convergence factor of WR and OWR and present for the first time an analysis for the optimized parameter in the transmission conditions for RC circuits of infinite length, a result which was announced in the short proceedings paper [23].

In WR methods, only the space domain or system of differential equations is split into multiple sub-domains or subsystems. One can further combine these WR methods with certain other time parallel methods, where the time domain is divided into multiple time subdomains. On each time subdomain of the WR method, Parareal [22,24] or the pipeline Schwarz waveform relaxation method [39], or Waveform Relaxation with Adaptive Pipelining (WRAP) [34], or Revisionist Integral Deferred Correction (RIDC) [10,38] can be considered. In the pipeline Schwarz waveform relaxation method and the WRAP method, WR iterates are computed in a pipeline manner to provide speedup and stability, while RIDC produces high order solutions in the same time as the lower order methods [10]. Further, multigrid WR methods [27,43] can also be implemented for parabolic differential equations.

WR methods are becoming popular for the simulation of field-circuit coupled problems. Such problems arises if one wants to look closely into the device. In this situation, a lumped circuit element is replaced by a PDE model. Another perspective for such problems comes from the practical use by the engineer, where different parts of a domain are not equally important and hence some of its properties can be neglected by replacing a part of it by a simple electric circuit, while in other parts the space–time discretization of the PDE is kept. Recently WR method were used for such field-circuit problems at CERN to simulate the quench protection system [4,26]. Moreover, if the RC circuits in the field-circuit coupled problem is divided into multiple sub-circuits, then the results obtained in our manuscript can be directly implemented in them. Further, OWR methods are also applied for the coupled electromagnetic field and power-electronic simulations [11].

We explain in Sect. 2 how one can obtain the mathematical model for the RC circuit of infinite length using MNA, and we show that the RC circuit is an approximation to the time dependent heat equation. In Sect. 3 we present and study the classical WR algorithm with overlap for RC circuits, and identify its convergence problems for low frequencies. In Sect. 4 we introduce the OWR with overlap for RC circuits. We give a circuit interpretation of the new transmission conditions, and also show that they can be interpreted as Robin transmission conditions for the associated heat equation. We then optimize the transmission conditions of OWR in Sect. 5 using asymptotic techniques. In Sect. 6 we show how to generalize our results to the many sub-circuit case. We perform some numerical tests to support our theoretical results in Sect. 7, and present our conclusions in Sect. 8.

2 Mathematical Model

We are interested in determining the voltages at the nodes of an RC circuit as in Fig. 1. To develop a mathematical model of this circuit, we use MNA, originally described by Ho et al. [29] in 1975. This technique produces a system of ODEs of the form $\dot{\mathbf{v}} = A\mathbf{v} + \mathbf{f}$, where the entries of the matrix A contain the elements of the circuit, $\mathbf{v}$ is the unknown vector of voltages at the nodes, and $\mathbf{f}$ contains the source terms. We now show how the matrix A is built using MNA, which is similar to the finite element assembly procedure [5].

In an electric circuit, any electric device with two terminals is called an element, and its terminals are called nodes. An electrical circuit is thus a system consisting of a set of elements and a set of nodes. The contribution of every element to the matrix equation is described by means of a template, called an element stamp [37]. Each element has a unique stamp which is given with the help of Kirchoff's Current Law (KCL) and Kirchoff's Voltage Law (KVL). For example, consider a resistor R placed between nodes with voltages v^+ and v^-, as shown in Fig. 2 (left). Let i be the current passing through it. Then using KCL, we have $i = v^+\left(\frac{1}{R}\right) - v^-\left(\frac{1}{R}\right)$. The corresponding element stamp is shown in Fig. 2 (right). The element stamp for a capacitor C is shown in Fig. 3.

To build the "descriptor system" form $M\dot{\mathbf{v}} = K\mathbf{v} + \tilde{\mathbf{f}}$, we start with a zero RHS vector $\tilde{\mathbf{f}} \in \mathbb{R}^N$, and zero matrices $M, K \in \mathbb{R}^{N\times N}$, where N is the number of nodes in the circuit. The vector $\mathbf{v}$ contains the unknown voltages at the nodes and remains unchanged throughout this process. We then read every element of the circuit one by one. As an element is read, its element stamp is added to the matrix M and K. Since the element stamp of a capacitor contains derivative terms, its element stamp is added to the matrix M, while the element stamp of a resistor is added in the matrix K. The independent current source term is stamped into the vector $\tilde{\mathbf{f}}$, see Fig. 4 for the element stamp of an independent current source. This process continues until all elements of the circuit are read and thus we obtain a system of differential equations in time of the form $\dot{\mathbf{v}} = A\mathbf{v} + \mathbf{f}$, where $A := M^{-1}K$ and $\mathbf{f} := M^{-1}\tilde{\mathbf{f}}$.

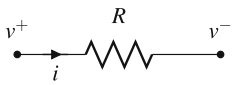

	v^+	v^-	RHS
v^+	$1/R$	$-1/R$	
v^-	$-1/R$	$1/R$	

Fig. 2 Element stamp for a resistor R

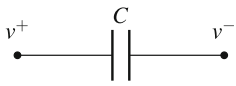

	v^+	v^-	RHS
v^+	$C\frac{d}{dt}$	$-C\frac{d}{dt}$	
v^-	$-C\frac{d}{dt}$	$C\frac{d}{dt}$	

Fig. 3 Element stamp for a capacitor C

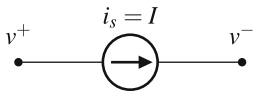

	v^+	v^-	RHS
v^+			-I
v^-			+I

Fig. 4 Element stamp for an independent current source

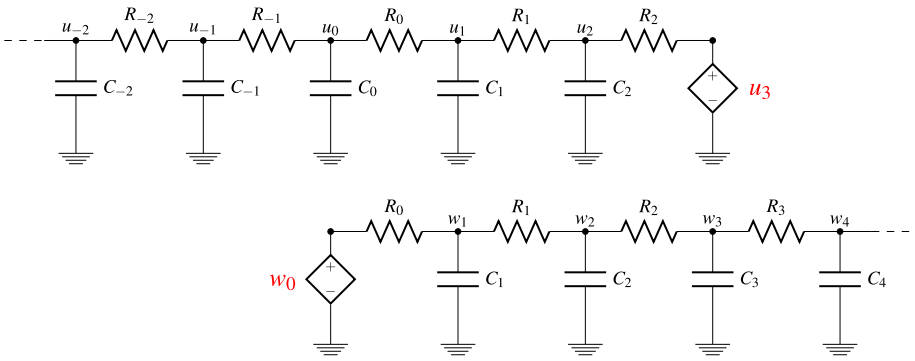

Fig. 5 Classical WR algorithm with 2 circuit nodes overlap

For the infinite RC circuit in Fig. 1, this system looks like

$$\frac{d\mathbf{v}}{dt} = \begin{bmatrix} \ddots & \ddots & \ddots & & & \\ & a_{-1} & b_0 & c_0 & & \\ & & a_0 & b_1 & c_1 & \\ & & & a_1 & b_2 & c_2 \\ & & & & \ddots & \ddots & \ddots \end{bmatrix} \mathbf{v} + \mathbf{f}, \tag{1}$$

where

$$a_i = \frac{1}{R_i C_{i+1}}, \quad b_i = -\left(\frac{1}{R_{i-1}} + \frac{1}{R_i}\right)\frac{1}{C_i}, \quad c_i = \frac{1}{R_i C_i}, \quad i \in \mathbb{Z},$$

and $\mathbf{f} = (I_s(t)/C_{-\infty}, 0, 0, \ldots, 0)^T$. This system of ODEs can also be viewed as semi-discretization by the method of lines of a heat equation in space–time: if we consider small resistors and capacitors, $R_i \approx \Delta x$ and $C_i \approx \Delta x$, then each equation of the system (1) takes the form

$$\frac{dv_i}{dt} = \frac{v_{i-1} - 2v_i + v_{i+1}}{\Delta x^2} + f_i, \tag{2}$$

and as $\Delta x \to 0$, we arrive at heat equation

$$\frac{\partial v}{\partial t} = \frac{\partial^2 v}{\partial x^2} + f. \tag{3}$$

Hence we can consider the RC circuit of infinite length as an approximation for the one dimensional heat equation on the unbounded domain $\Omega_x = (-\infty, \infty)$.

For a short vector $\mathbf{v}$, one can solve the system of ODEs (1) by simple discretization and matrix manipulation. However if the size of the vector $\mathbf{v}$ is in the millions and for more complicated circuits, solving the system (1) is computationally costly, and one needs parallel methods. One such method is WR as we now show.

3 The WR Algorithm

For a general WR algorithm, one decomposes the system (1) into many sub-systems, but to understand the key features of WR, we consider a decomposition into two sub-systems

only. We decompose the infinite RC circuit from Fig. 1 at node 0 into two equal sub-circuits, and motivated by the PDE relation shown in (3) and the Schwarz WR algorithms studied in [13,17] which use overlap, we include an overlap of n nodes in the first sub-circuit. Let us denote the first sub-system unknowns by $\mathbf{u(t)}$ and the second sub-system unknowns by $\mathbf{w(t)}$, $\mathbf{u(t)} := (\ldots, u_{-1}, u_0, \ldots, u_n)^T = (\ldots, v_{-1}, v_0, \ldots, v_n)^T$ and $\mathbf{w(t)} := (w_1, w_2, \ldots)^T = (v_1, v_2, \ldots)^T$. Figure 5 shows the decomposition of the circuit when two nodes are in the overlap. We see that when we decompose the circuit, we need to add a voltage source u_3 in the first sub-circuit and w_0 in the second. At each iteration k, these voltage sources are given by transmission conditions which transfer information between the sub-circuits. The system of differential equations for the decomposed sub-circuits are

$$\begin{aligned}
\dot{\mathbf{u}}^{k+1}(t) &= \begin{bmatrix} \ddots & \ddots & \ddots & \\ & a_{n-2} & b_{n-1} & c_{n-1} \\ & & a_{n-1} & b_n \end{bmatrix} \begin{bmatrix} \vdots \\ u_{n-1}(t) \\ u_n(t) \end{bmatrix}^{k+1} + \begin{bmatrix} \vdots \\ 0 \\ c_n u_{n+1}(t) \end{bmatrix}^{k+1} + \begin{bmatrix} \vdots \\ f_{n-1} \\ f_n \end{bmatrix}, \\
\dot{\mathbf{w}}^{k+1}(t) &= \begin{bmatrix} b_1 & c_1 & & \\ a_1 & b_2 & c_2 & \\ & \ddots & \ddots & \ddots \end{bmatrix} \begin{bmatrix} w_1(t) \\ w_2(t) \\ \vdots \end{bmatrix}^{k+1} + \begin{bmatrix} a_0 w_0(t) \\ 0 \\ \vdots \end{bmatrix}^{k+1} \begin{bmatrix} f_1 \\ f_2 \\ \vdots \end{bmatrix},
\end{aligned} \tag{4}$$

where the unknowns $u_{n+1}^{k+1}(t)$ and $w_0^{k+1}(t)$ are determined by the transmission conditions

$$u_{n+1}^{k+1}(t) = w_{n+1}^k(t), \qquad w_0^{k+1}(t) = u_0^k(t). \tag{5}$$

We see that at each iteration, these transmission conditions transfer voltages at the interface. Comparing this with Schwarz WR applied to PDEs in [13,17], these conditions can be interpreted as Dirichlet boundary conditions.

To start the algorithm, we specify an initial guess for the solution $w_{n+1}^0(t)$ and $u_0^0(t)$, and then solve the sub-systems (4) for all time $t \in (0, T]$. Note that the two sub-systems can be solved in parallel, since in the transmission conditions (5) the two sub-systems use both data from the previous iteration, like in a block Jacobi method [41] from linear algebra. One could also do the solves sequentially, and use the newest value available in the second transmission condition, $w_0^{k+1}(t) = u_0^{k+1}(t)$, which would be more like a block Gauss Seidel iteration from linear algebra, but the convergence analysis is similar, so we will focus on the parallel version here.

3.1 Convergence Analysis of the Classical WR Algorithm

The presence of different resistors R_i and capacitors C_i makes the convergence analysis difficult, so to simplify, we assume that all resistors and capacitors have the same value, i.e. $R_i := R$ and $C_i := C$ for all $i \in \mathbb{Z}$ which leads to $a_i = a$, $b_i = b$ and $c_i = a$ for all $i \in \mathbb{Z}$, where $a := \frac{1}{RC}$ and $b := \frac{-2}{RC}$.

We study the convergence of the WR algorithm (4) with transmission conditions (5) using the Laplace transform:

Definition 3.1 If $f(t)$ is a real or complex valued function of the non-negative real variable t, then the Laplace transform is defined by the integral

$$\mathcal{L}(s) = \hat{f}(s) := \int_0^\infty e^{-st} f(t) dt, \qquad s \in \mathbb{C}.$$

The Laplace transform transforms the system of differential equations in time into a system of algebraic equations which are easier to analyze, and is very useful to study WR algorithms, see e.g. [9,16,30,31] and references therein. Further since the system (4) is linear, the error equations correspond to the homogeneous problem, $\mathbf{f} = 0$, with zero initial conditions, $\mathbf{u}^{k+1}(0) = \mathbf{w}^{k+1}(0) = 0$. The Laplace transform allows us to show that $\hat{u}_j^{k+1}(s) = \rho_{n,cla}(s)\hat{u}_j^{k-1}(s)$ and $\hat{w}_j^{k+1}(s) = \rho_{n,cla}(s)\hat{w}_j^{k-1}(s)$, where $\hat{u}_j^k$ and $\hat{w}_j^k$ are the Laplace transforms of u_j^k and w_j^k, and $\rho_{n,cla}(s)$ is the convergence factor. We can then use the Parseval equality for $s = \sigma + i\omega, \sigma \geq 0$, to obtain a convergence estimate in the weighted L^2 norm $\|x(t)\|_\sigma := \|e^{-\sigma t}x(t)\|_{L^2}$,

$$\begin{aligned} \|u_j^{2k}(t)\|_\sigma &\leq \left(\sup_{\omega\in\mathbb{R}} \left|\rho_{n,cla}(\sigma + i\omega)\right|\right)^k \|u_j^0(t)\|_\sigma, \\ \|w_j^{2k}(t)\|_\sigma &\leq \left(\sup_{\omega\in\mathbb{R}} \left|\rho_{n,cla}(\sigma + i\omega)\right|\right)^k \|w_j^0(t)\|_\sigma. \end{aligned} \tag{6}$$

Convergence in Laplace space with a convergence factor $\rho_{n,cla}(s)$ less than one implies convergence in the time domain in the weighted norm $\|\cdot\|_\sigma$, and for $\sigma = 0$, we obtain convergence in L^2.

We now find a closed form for the convergence factor $\rho_{n,cla}$. The Laplace transform for $s \in \mathbb{C}$ of the WR algorithm (4) is given by

$$\begin{aligned} s\hat{\mathbf{u}}^{k+1} &= \begin{bmatrix} \ddots & \ddots & \ddots & \\ & a & b & a \\ & & a & b \end{bmatrix} \begin{bmatrix} \vdots \\ \hat{u}_{n-1} \\ \hat{u}_n \end{bmatrix}^{k+1} + \begin{bmatrix} \vdots \\ 0 \\ a\hat{w}_{n+1}^k \end{bmatrix}, \\ s\hat{\mathbf{w}}^{k+1} &= \begin{bmatrix} b & a & & \\ a & b & a & \\ & \ddots & \ddots & \ddots \end{bmatrix} \begin{bmatrix} \hat{w}_1 \\ \hat{w}_2 \\ \vdots \end{bmatrix}^{k+1} + \begin{bmatrix} a\hat{u}_0^k \\ 0 \\ \vdots \end{bmatrix}, \end{aligned} \tag{7}$$

where we have already included the transmission conditions (5); this shows the dependence of $\hat{\mathbf{u}}$ on $\hat{\mathbf{w}}$ and vice-versa. Solving the sub-systems (7) requires solving a recurrence relation of the form $ay_{j-1} + (b-s)y_j + ay_{j+1} = 0$, where $y_j = \hat{u}_j^{k+1}$, $\hat{w}_j^{k+1}$ for $j \in \mathbb{Z}$. In order to find the convergence factor of the WR algorithm, we need the following lemma.

Lemma 1 *Let $a > 0$, $b < 0$, $i = \sqrt{-1}$, and $s := \sigma + i\omega$, with $\sigma \geq 0$. For $-b \geq 2a$, the roots $\lambda_{1,2} := \frac{s-b\pm\sqrt{(b-s)^2-4a^2}}{2a}$ of the characteristic equation $ay_{j-1} + (b-s)y_j + ay_{j+1} = 0$ of the sub-systems in (7) satisfy $|\lambda_2| \leq 1 \leq |\lambda_1|$.*

Proof The proof of this lemma can be found in [23]. □

Theorem 1 *The convergence factor $\rho_{n,cla}$ of the classical WR algorithm (7) with n nodes overlap for an RC circuit of infinite length is given by*

$$\rho_{n,cla}(s) = \left(\frac{1}{\lambda_1^2}\right)^{n+1}. \tag{8}$$

Proof The detailed proof of this theorem can be found in [23], but for completeness, we present a brief sketch of the proof. Solving the recurrence relation $ay_{j-1}+(b-s)y_j+ay_{j+1} = 0$ for $y_j = \hat{u}_j^{k+1}$ gives $\hat{u}_j^{k+1} = A^{k+1}\lambda_1^j$ for $j = (\ldots, n-2, n-1, n)$, and for $y_j = \hat{w}_j^{k+1}$

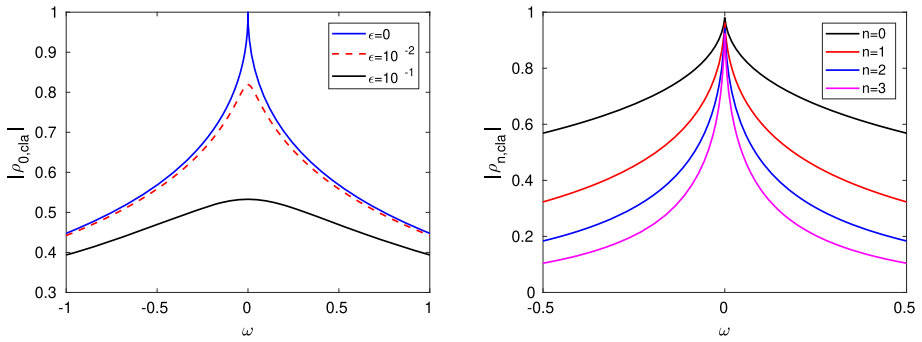

Fig. 6 Convergence factor for $s = i\omega$ for $n = 0$ and different values of ϵ (left) and for different overlaps with $\epsilon = 1e-4$ (right)

we get $\hat{w}_j^{k+1} = D^{k+1}\lambda_2^j$ for $j \in \mathbb{N}$, with λ_1 and λ_2 defined in Lemma 1. The transmission conditions (5) determine the constants A^{k+1} and B^{k+1} and we find

$$\begin{aligned} \hat{u}_j^{k+1} &= \left(\frac{-a}{a\lambda_1^{-1} + (b-s)}\right)\left(\frac{\hat{w}_{n+1}^k}{\lambda_1^n}\right)\lambda_1^j \qquad \text{for } j = \ldots, n-2, n-1, n, \\ \hat{w}_j^{k+1} &= \left(\frac{-a\hat{u}_0^k}{(b-s) + a\lambda_2}\right)\lambda_2^{j-1} \qquad \text{for } j \in \mathbb{N}. \end{aligned} \tag{9}$$

The above expression together with Vieta's formulas $\lambda_1 + \lambda_2 = (s-b)/a$ and $\lambda_1\lambda_2 = 1$ gives $\hat{u}_j^{k+1} = \rho_{n,cla}(s)\hat{u}_j^{k-1}$ for $j = (\ldots, n-1, n)$ and $\hat{w}_j^{k+1} = \rho_{n,cla}(s)\hat{w}_j^{k-1}$ for $j \in \mathbb{N}$ where $\rho_{n,cla}(s)$ is given in (8). □

From Lemma 1, we see that if $|b| = 2a$ and $s = 0$, the convergence factor $|\rho_{n,cla}(0)| = 1$, while for $b = -(2+\epsilon)a$ with $\epsilon > 0$, we have $|\rho_{n,cla}(s)| < 1$. It is therefore interesting to study the case $\epsilon > 0$ and then analyze the limit as $\epsilon \to 0$. In fact, in this limit, the rate of convergence deteriorates at $\omega = 0$, as we show on the left in Fig. 6. We also show on the right in Fig. 6 that increasing the overlap increases the rate of convergence, but the effect is very small for ω close to zero when $s = i\omega$.

For circuits, the introduction of ϵ leads to the addition of a resistor $\tilde{R} = R/\epsilon$ at each node of the circuit (see Fig. 7). The inclusion of the resistors $\tilde{R}$ presents a practical case where there is a small leakage of current in the dielectric element. The limit $\epsilon \to 0$ leads to the limit $\tilde{R} \to \infty$, which means that no current passes through these resistors and hence the resistors $\tilde{R}$ can be removed from the circuit. Thus with the limit $\epsilon \to 0$, the circuit in Fig. 7 is a good approximation to the circuit in Fig. 5.

4 OWR Algorithm

The main drawback of the classical WR algorithm is that it is very slow especially when large time windows are used. Large time windows in real space correspond to small frequencies ω in $s = \sigma + i\omega$ in Laplace space. When $\epsilon \to 0$ with $b = -(2+\epsilon)a$, we observe that $|\rho_{n,cla}(0)| \to 1$, which means the convergence rate slows down for small ω, and increasing the overlap does mostly improve the convergence of higher frequencies ω, as one can see in Fig. 6 on the right. The Dirichlet transmission conditions (5) which exchange just voltages

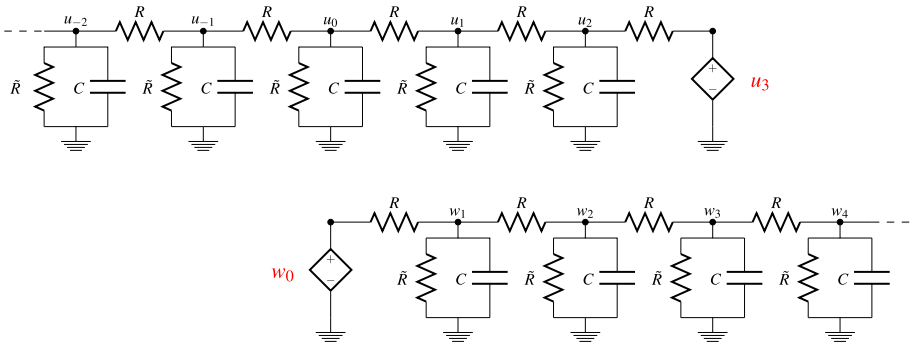

Fig. 7 WR algorithm with $b = -(2+\epsilon)a$ and $\tilde{R} = R/\epsilon$

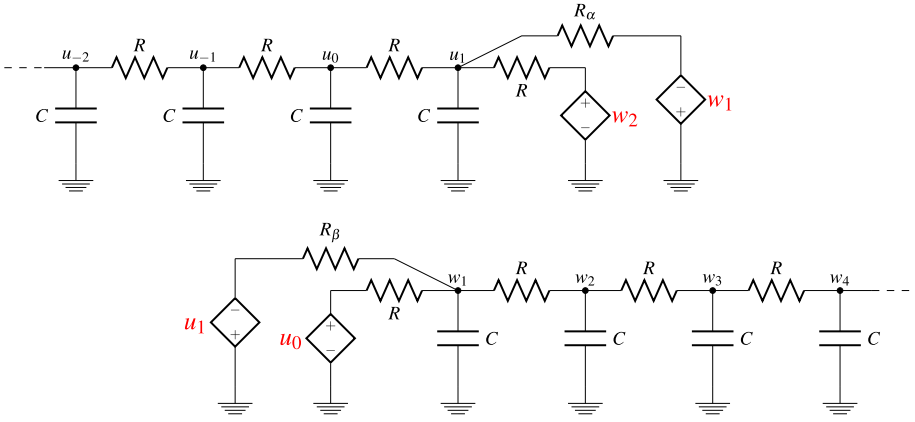

Fig. 8 OWR algorithm with 1 circuit node overlap with $R_\alpha := R(1+\alpha)$ and $R_\beta = R(1-\beta)$

at the interfaces are the main reason for this slow convergence. We thus search for better transmission conditions to exchange information between the sub-circuits. One way is to use optimized transmission conditions, which are defined for this RC circuit in [23] as

$$\begin{aligned}(u_{n+1}^{k+1} - u_n^{k+1}) + \alpha u_{n+1}^{k+1} &= (w_{n+1}^k - w_n^k) + \alpha w_{n+1}^k,\\ (w_1^{k+1} - w_0^{k+1}) + \beta w_0^{k+1} &= (u_1^k - u_0^k) + \beta u_0^k,\end{aligned} \tag{10}$$

where $\alpha, \beta \in \mathbb{R}$ and k is the iteration index. These transmission conditions exchange both voltages and currents at the interface, which can be seen by dividing the first equation by α and the second by β. The term $\frac{u_{n+1}^{k+1} - u_n^{k+1}}{\alpha}$ can be viewed as a current and u_{n+1}^{k+1} is a voltage. These transmission conditions are called optimized transmission conditions since we need to find the best (optimized) values for α and β such that the convergence factor is as small as possible.

For circuits, the introduction of the new transmission conditions (10) means two voltage sources need to be added at the interface of each sub-circuit. From Fig. 8, we see that the resistors $R_\alpha := R(1+\alpha)$ and $R_\beta := R(1-\beta)$, which depend on the parameters α and β, are added. Once these constants α and β are found, one can substitute them to find resistors R_α and R_β and can be used at the interface. Similar to the WR algorithm, at each iteration the voltage sources w_3, w_2, u_0, u_1 are transferred between the sub-circuits.

We can also interpret the new transmission conditions (10) as Robin transmission conditions for the discretized heat equation (2): if we divide the first equation of (10) by $\bar{\alpha} := \frac{\alpha}{p}$ for some $p > 0$ and the second equation by $\bar{\beta} := \frac{-\beta}{p}$, we obtain

$$\frac{u_{n+1}^{k+1} - u_n^{k+1}}{\bar{\alpha}} + p u_{n+1}^{k+1} = \frac{w_{n+1}^{k} - w_n^{k}}{\bar{\alpha}} + p w_{n+1}^{k},$$
$$\frac{w_1^{k+1} - w_0^{k+1}}{\bar{\beta}} - p w_0^{k+1} = \frac{u_1^{k} - u_0^{k}}{\bar{\beta}} - p u_0^{k}.$$

If we consider now $\bar{\alpha} \approx \Delta x$ and $\bar{\beta} \approx \Delta x$, then the fractions inside the above equations represent discretization for the derivative $\frac{\partial u}{\partial x}$ and $\frac{\partial w}{\partial x}$, and we thus obtain in the limit Robin transmission conditions,

$$\left(\frac{\partial}{\partial x} + p\right) u_{n+1}^{k+1} = \left(\frac{\partial}{\partial x} + p\right) w_{n+1}^{k},$$
$$\left(\frac{\partial}{\partial x} - p\right) w_0^{k+1} = \left(\frac{\partial}{\partial x} - p\right) u_0^{k}.$$

4.1 Convergence of OWR

As for the classical WR algorithm, we analyze the convergence of the OWR algorithm in Laplace space. We first rearrange the optimized transmission conditions as

$$u_{n+1}^{k+1} = \frac{u_n^{k+1}}{1+\alpha} + w_{n+1}^{k} - \frac{w_n^{k}}{1+\alpha},$$
$$w_0^{k+1} = -\frac{w_1^{k+1}}{\beta - 1} + u_0^{k} + \frac{u_1^{k}}{\beta - 1}, \tag{11}$$

where all the voltages u_i and w_i depend on time t. We substitute these rearranged transmission conditions into (4) and take the Laplace transform to arrive at

$$\begin{aligned} s\hat{\mathbf{u}}^{k+1} &= \begin{bmatrix} \ddots & \ddots & \ddots & & \\ & a & b & a & \\ & & a & b + \frac{a}{\alpha+1} \end{bmatrix} \begin{bmatrix} \vdots \\ \hat{u}_{n-1} \\ \hat{u}_n \end{bmatrix}^{k+1} + \begin{bmatrix} \vdots \\ 0 \\ a\hat{w}_{n+1}^{k} - \frac{a}{\alpha+1}\hat{w}_n^{k} \end{bmatrix}, \\ s\hat{\mathbf{w}}^{k+1} &= \begin{bmatrix} b - \frac{a}{\beta-1} & a & & \\ a & b & a & \\ & \ddots & \ddots & \ddots \end{bmatrix} \begin{bmatrix} \hat{w}_1 \\ \hat{w}_2 \\ \vdots \end{bmatrix}^{k+1} + \begin{bmatrix} a\hat{u}_0^{k} + \frac{a}{\beta-1}\hat{u}_1^{k} \\ 0 \\ \vdots \end{bmatrix}. \end{aligned} \tag{12}$$

We need to give initial guesses $\hat{w}_{n+1}^0$, $\hat{w}_n^0$, $\hat{u}_0^0$ and $\hat{u}_1^0$ to start this algorithm.

Theorem 2 *The convergence factor $\rho_n(s, \alpha, \beta)$ of the OWR algorithm (12) for an RC circuit of infinite length is given by*

$$\rho_n(s, \alpha, \beta) = \left(\frac{\alpha + 1 - \lambda_1}{\lambda_1(1+\alpha) - 1}\right)\left(\frac{\lambda_1 + \beta - 1}{1 + (\beta - 1)\lambda_1}\right)\left(\frac{1}{\lambda_1^2}\right)^n. \tag{13}$$

Proof To find the convergence factor, we proceed as in the proof of Theorem 1 to arrive at $\hat{u}_j^{k+1} = A^{k+1}\lambda_1^j$ for $j = (\ldots, n-1, n)$, and $\hat{w}_j^{k+1} = D_j^{k+1}\lambda_2^j$ for $j \in \mathbb{N}$. To determine the

constants A^{k+1} and D^{k+1}, we use the optimized transmission conditions (11) and get

$$A^{k+1} = B^k \left(\frac{\lambda_2(1+\alpha)-1}{\lambda_1(1+\alpha)-1}\right)\left(\frac{\lambda_2}{\lambda_1}\right)^n, \quad B^{k+1} = A^k \left(\frac{\lambda_1+\beta-1}{\lambda_2+\beta-1}\right). \tag{14}$$

Using $\lambda_1\lambda_2 = 1$ and Eq. (14), we arrive at

$$\begin{aligned}
\hat{u}_j^{k+1} &= A^{k+1}\lambda_1^j \qquad j \in (\ldots, -2, -1, 0, 1, \ldots, n) \\
&= \left(\frac{\lambda_2(1+\alpha)-1}{\lambda_1(1+\alpha)-1}\right)\left(\frac{\lambda_1+\beta-1}{\lambda_2+\beta-1}\right)\left(\frac{\lambda_2}{\lambda_1}\right)^n A^{k-1}\lambda_1^j \\
&= \left(\frac{\alpha+1-\lambda_1}{\lambda_1(1+\alpha)-1}\right)\left(\frac{\lambda_1+\beta-1}{1+(\beta-1)\lambda_1}\right)\left(\frac{1}{\lambda_1^2}\right)^n \hat{u}_j^{k-1} \\
&= \rho_n(s,\alpha,\beta)\hat{u}_j^{k-1},
\end{aligned}$$

where the convergence factor $\rho_n(s,\alpha,\beta)$ is given by (13). Similarly, we can also show that $\hat{w}_j^{k+1} = \rho_n(s,\alpha,\beta)\hat{w}_j^{k-1}$, for $j \in \mathbb{N}$, and this completes the proof. □

Lemma 2 *If $\alpha > 0$, $\beta < 0$, and $\epsilon > 0$, then the modulus of the convergence factor $\rho_n(s,\alpha,\beta)$ of the OWR algorithm is less than 1, that is, $|\rho_n(s,\alpha,\beta)| < 1$ for all $n \geq 0$.*

Proof Since $\lambda_1 \in \mathbb{C}$, we assume $\lambda_1 = x + iy$. Lemma 1 states that for $\epsilon > 0$, where $b = -(2+\epsilon)a$, we have $|\lambda_1| > 1$ and hence $x^2+y^2 > 1$. Further for $\alpha > 0$, $(\alpha+1)^2-1 > 0$ and hence

$$\begin{aligned}
&(\alpha+1)^2 - 1 < [(\alpha+1)^2 - 1](x^2+y^2) \\
&\iff (\alpha+1)^2 + x^2 + y^2 < (\alpha+1)^2x^2 + (\alpha+1)^2y^2 + 1 \\
&\iff (\alpha+1)^2 + x^2 + y^2 - 2x(\alpha+1) < (\alpha+1)^2x^2 + (\alpha+1)^2y^2 + 1 - 2x(\alpha+1) \\
&\iff (\alpha+1-x)^2 + y^2 < ((\alpha+1)x-1)^2 + (\alpha+1)^2y^2 \\
&\iff |\alpha+1-x-iy| < |(\alpha+1)(x+iy)-1|.
\end{aligned}$$

Similarly, for $\beta < 0$, we can show $|\lambda_1+\beta-1| < |1+(\beta-1)\lambda_1|$ and this completes the proof. □

We observe from (13) that the effect of overlap on the convergence factor given by $\left(\frac{1}{\lambda_1^2}\right)^n$ is the same for both the WR and the OWR algorithm. This means increasing the overlap increases the rate of convergence also for OWR. The convergence factor is also the same for all the circuit nodes irrespective of which sub-circuit they belong to. Further, for fast convergence, we would like to have the convergence factor $|\rho_n(s,\alpha,\beta)|$ as small as possible. The parameters a, b represent circuit elements and cannot be changed, but we can choose α and β such that $|\rho_n(s,\alpha,\beta)|$ becomes as small as possible. So what is the best possible choice for the parameters α and β?

Theorem 3 *For the circuit decomposition into two sub-circuits with only one interface, the Optimized Waveform Relaxation method converges in two iterations, independently of initial guess and the overlap, if*

$$\alpha_{opt} := \lambda_1 - 1 \quad \text{and} \quad \beta_{opt} := 1 - \lambda_1. \tag{15}$$

Proof Setting the convergence factor $\rho_n(s,\alpha,\beta) = 0$, we find $\alpha = \lambda_1 - 1$ and $\beta = 1 - \lambda_1$. Since, $\hat{u}_j^{k+1} = \rho_n(s,\alpha,\beta)\hat{u}_j^{k-1}$ and $\hat{w}_j^{k+1} = \rho_n(s,\alpha,\beta)\hat{w}_j^{k-1}$, we have $\hat{u}_j^2$ and $\hat{w}_j^2$ identically zero and hence the OWR has converged in two iterations. □

One can see that this is the best choice, since the solution in each sub-system depends on all the source terms f_j and during the first iteration, each sub-system uses only the local f_j to compute the approximation. It is only for the second iteration that information is transferred. Therefore, convergence cannot be achieved in less than 2 iterations.

Since λ_1 is a complicated function of $s \in \mathbb{C}$, its inverse Laplace transform leads to non local operators in time for α_{opt} and β_{opt}. These non local operators are expensive to use since they require convolution operations. It is therefore of interest to approximate α_{opt} and β_{opt} by a polynomial in s. In this paper, we will focus on approximation of α_{opt} and β_{opt} by a constant.

5 Optimization

Mathematically, we want $|\rho_n(s, \alpha, \beta)| \ll 1$, which leads to solving the min-max problem

$$\min_{\alpha,\beta} \left(\max_{s} |\rho_n(s, \alpha, \beta)| \right). \tag{16}$$

Since $s \in \mathbb{C}$ with $s = \sigma + i\omega$, the above optimization problem is in four variables and hence already very difficult to solve. We simplify the problem further using some assumptions and the following lemmas.

Lemma 3 *For $\alpha > 0$, $\beta < 0$, the maximum of $|\rho_n(s, \alpha, \beta)|$ lies on the imaginary axis of the complex plane.*

Proof The detailed proof of this lemma can be found in [23]. The idea is to show that $\rho_n(s, \alpha, \beta)$ is analytic in the right half of the complex plane and then to use the maximum modulus principle for analytic functions. □

Lemma 4 *For $\sigma = 0$, $|\rho_n(\omega, \alpha, \beta)|$ is symmetric in ω.*

Proof On the imaginary axis of the complex plane, $\sigma = 0$, and hence from the definition of λ_1, we get

$$\lambda_1(\omega) = \frac{i\omega - b + \sqrt{(i\omega - b)^2 - 4a^2}}{2a} = \frac{i\omega + (2+\epsilon)a + \sqrt{r + ip}}{2a},$$

where $r := \epsilon^2 a^2 - \omega^2 + 4\epsilon a^2$ and $p := 2(2+\epsilon)\omega a$. Further, letting $z_1 + iz_2 := \sqrt{r + ip}$, where $z_1, z_2 \in \mathbb{R}$, we get $\lambda_1(\omega) = x + iy = \frac{(2+\epsilon)a + z_1}{2a} + i\frac{\omega + z_2}{2a}$. One can check that if $\sqrt{r + ip} = z_1 + iz_2$ then $\sqrt{r - ip} = z_1 - iz_2$. Therefore, $\lambda_1(-\omega) = \frac{(2+\epsilon)a + z_1}{2a} - i\frac{\omega + z_2}{2a}$ which shows that $\overline{\lambda_1(-\omega)} = \lambda_1(\omega)$. Now,

$$\begin{aligned}
|\rho_n(-\omega, \alpha, \beta)| &= \left| \left(\frac{\alpha + 1 - \lambda_1(-\omega)}{[\lambda_1(-\omega)](1+\alpha) - 1} \right) \left(\frac{\lambda_1(-\omega) + \beta - 1}{1 + (\beta - 1)[\lambda_1(-\omega)]} \right) \left(\frac{1}{[\lambda_1(-\omega)]^2} \right)^n \right| \\
&= \left| \left(\overline{\frac{\alpha + 1 - \lambda_1(\omega)}{[\lambda_1(\omega)](1+\alpha) - 1}} \right) \right| \left| \left(\overline{\frac{\lambda_1(\omega) + \beta - 1}{1 + (\beta - 1)[\lambda_1(\omega)]}} \right) \right| \left| \left(\overline{\frac{1}{[\lambda_1(\omega)]^2}} \right)^n \right| \\
&= \left| \left(\frac{\alpha + 1 - \lambda_1(\omega)}{[\lambda_1(\omega)](1+\alpha) - 1} \right) \right| \left| \left(\frac{\lambda_1(\omega) + \beta - 1}{1 + (\beta - 1)[\lambda_1(\omega)]} \right) \right| \left| \left(\frac{1}{[\lambda_1(\omega)]^2} \right)^n \right| \\
&= |\rho_n(\omega, \alpha, \beta)|,
\end{aligned}$$

which concludes the proof. □

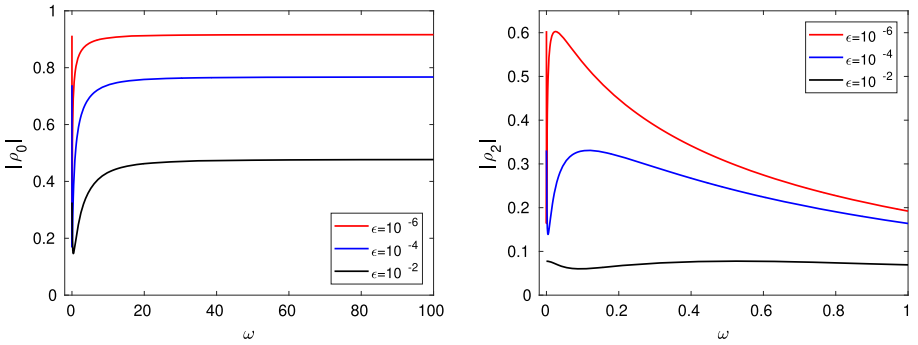

Fig. 9 Equi-oscillation for different values of ϵ for $n = 0$ (left) and for $n = 2$ (right)

From Theorem 3, we observe that α_{opt} and β_{opt} are related to each other via the relation $\beta_{opt} = -\alpha_{opt}$, which suggests the natural assumption $\beta = -\alpha$. In our RC circuit of infinite length, this would mean that at the interface (where the circuit is split into two), the current flowing in both sub-circuits is equal but into opposite direction. This interpretation is easy to see for the non-overlapping case $n = 0$. Recall that the terms $\frac{u_{n+1}^{k+1} - u_n^{k+1}}{\alpha}$ and $\frac{w_1^{k+1} - w_0^{k+1}}{\beta}$ are viewed as currents. Thus with $\beta = -\alpha$, their values are same but their sign is opposite.

Lemmas 3 and 4 state that the min-max problem (16) needs to be solved for $s = i\omega$, $\omega \geq 0$. However, for numerical calculations, we consider the time $t \in [0, T]$, and also a discretization with Δt as the discretization parameter. Hence $\omega_{min} \leq \omega \leq \omega_{max}$, where we can estimate $\omega_{min} = \frac{\pi}{T}$ and $\omega_{max} = \frac{\pi}{\Delta t}$. Note that $\omega_{min} > 0$, but to further simplify our analysis, we consider a wider range for ω, that is, $\omega \in [0, \omega_{max}]$. Therefore, our min-max problem (16) reduces to

$$\min_{\alpha} \left(\max_{0 \leq \omega \leq \omega_{max}} |\rho_n(\omega, \alpha, -\alpha)| \right). \tag{17}$$

We observe numerically, see Fig. 9, that the solution for the min-max problem (17) is given by equi-oscillation. However the behavior of equi-oscillation is different for the non-overlapping and overlapping case. We first analyze the non-overlapping case, that is, $n = 0$, where the equi-oscillation occurs for $\omega = 0$ and $\omega = \omega_{max} \to \infty$ (see the left plot of Fig. 9). This means the optimized α denoted by α_0^* satisfies

$$|\rho_0(0, \alpha_0^*)| = |\rho_0(\infty, \alpha_0^*)|, \tag{18}$$

where we have dropped the parameter $-\alpha$ for simplicity, $\rho_n(\omega, \alpha) := \rho_n(\omega, \alpha, -\alpha)$.

To start with, we find the explicit expression for $|\rho_0(\omega, \alpha)|$. In the proof of Lemma 4, we expressed $\lambda_1 = x + iy$, where $x = \frac{(2+\epsilon)a + z_1}{2a}$ and $y = \frac{\omega + z_2}{2a}$ and hence

$$|\rho_0(\omega, \alpha)| = \frac{|\alpha + 1 - \lambda_1|^2}{|(1+\alpha)\lambda_1 - 1|^2} =: \frac{A(\omega, \alpha)}{B(\omega, \alpha)}, \tag{19}$$

where

$$A(\omega, \alpha) = |\alpha + 1 - \lambda_1|^2 = \alpha^2 + x^2 + 1 + y^2 - 2x - 2x\alpha + 2\alpha,$$
$$B(\omega, \alpha) = |(1+\alpha)\lambda_1 - 1|^2 = y^2 + 1 - 2x + 2\alpha y^2 - 2x\alpha + 2\alpha x^2 + x^2 + y^2\alpha^2 + x^2\alpha^2.$$

$A(\omega, \alpha)$ and $B(\omega, \alpha)$ are complicated functions of ω and α which makes the analysis difficult. To simplify, we use asymptotic analysis to find an explicit expression for α_0^*. We first express

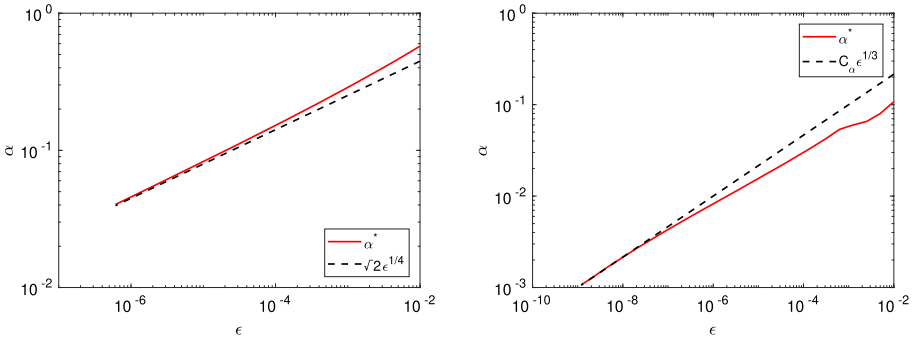

Fig. 10 Dependence of α^* on ϵ for $n = 0$ (left) and with $C_\alpha = \left(\frac{1}{n}\right)^{1/3}$ for $n = 1$ (right)

$|\rho_0(0,\alpha)|$ and $|\rho_0(\infty,\alpha)|$ as polynomials in ϵ using the ansatz $\alpha = C_\alpha\epsilon^\delta$, where $\epsilon = -\frac{b}{a} - 2$ and $\delta > 0$. The dependence of α_0^* on ϵ for $n = 0$ is illustrated numerically in the left plot of Fig. 10.

Lemma 5 *For the non-overlapping case, $n = 0$, and for small $\epsilon > 0$, the modulus of the convergence factor $|\rho_0(\omega,\alpha)|$ for the OWR algorithm for $\omega = 0$ and $\omega \to \infty$ is given by*

$$|\rho_0(0,\alpha)| = 1 - \frac{4}{C_\alpha}\epsilon^{\frac{1}{2}-\delta} + \mathcal{O}(\epsilon^{1-2\delta}) \tag{20}$$

and

$$|\rho_0(\infty,\alpha)| = 1 - 2C_\alpha\epsilon^\delta + \mathcal{O}(\epsilon^{2\delta}). \tag{21}$$

Proof We first find asymptotic expressions for x and y which are functions of ω. From the expression of $\lambda_1(\omega) = \frac{i\omega - b + \sqrt{(i\omega-b)^2 - 4a^2}}{2a}$, substituting $\omega = 0$, $b = -(2+\epsilon)a$ and using a Taylor expansion for $(1+\epsilon)^{1/2} = 1 + \frac{\epsilon}{2} - \frac{\epsilon^2}{8} + \mathcal{O}(\epsilon^3)$ gives

$$\lambda_1(0) = \frac{2+\epsilon}{2} + \frac{\sqrt{4\epsilon+\epsilon^2}}{2} = 1 + \frac{\epsilon}{2} + \epsilon^{1/2}\sqrt{1+\frac{\epsilon}{4}} = 1 + \epsilon^{1/2} + \frac{\epsilon}{2} + \mathcal{O}(\epsilon^{3/2}).$$

Thus we have $x = 1 + \epsilon^{1/2} + \frac{\epsilon}{2} + \mathcal{O}(\epsilon^{3/2})$ and $y = 0$. Using the ansatz $\alpha = C_\alpha\epsilon^\delta$, we arrive at $A(0,\alpha) = C_\alpha^2\epsilon^{2\delta} - 2C_\alpha\epsilon^{\delta+1/2} + \epsilon + \mathcal{O}(\epsilon^{\delta+1})$ and similarly, $B(0,\alpha) = C_\alpha^2\epsilon^{2\delta} + 2C_\alpha\epsilon^{\delta+1/2} + 2C_\alpha^2\epsilon^{2\delta+1/2} + \mathcal{O}(\epsilon)$. Therefore,

$$\begin{aligned}
|\rho_0(0,\alpha)| = \frac{A(0,\alpha)}{B(0,\alpha)} &= \frac{1 - \frac{2}{C_\alpha}\epsilon^{1/2-\delta} + \frac{1}{C_\alpha^2}\epsilon^{1-2\delta} + \mathcal{O}(\epsilon^{1-\delta})}{1 + \frac{2}{C_\alpha}\epsilon^{1/2-\delta} + 2\epsilon^{1/2} + \mathcal{O}(\epsilon^{1-2\delta})} \\
&= \left(1 - \frac{2}{C_\alpha}\epsilon^{1/2-\delta} + \frac{\epsilon^{1-2\delta}}{C_\alpha^2} + \mathcal{O}(\epsilon^{1-\delta})\right)\left(1 - \frac{2}{C_\alpha}\epsilon^{1/2-\delta} + \frac{2\epsilon^{1-2\delta}}{C_\alpha^2} + \mathcal{O}(\epsilon^{1/2})\right) \\
&= 1 - \frac{4}{C_\alpha}\epsilon^{1/2-\delta} + \mathcal{O}(\epsilon^{1/2}).
\end{aligned}$$

Since $\lim_{\omega\to\infty}\lambda_1(\omega) = \infty$, it is easier to find an expression for $|\rho_0(\infty,\alpha)|$ which can be rewritten as

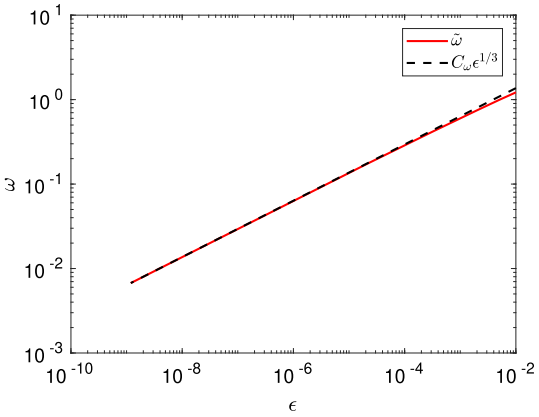

Fig. 11 Dependence of $\tilde{\omega}$ on ϵ with $C_\omega = \frac{2a}{n}\left(\frac{1}{n}\right)^{1/3}$

$$|\rho_0(\infty,\alpha)| = \lim_{\omega\to\infty}\frac{A(\omega,\alpha)}{B(\omega,\alpha)} = \lim_{\omega\to\infty}\left|\frac{\frac{\alpha+1}{\lambda_1(\omega)}-1}{1+\alpha-\frac{1}{\lambda_1(\omega)}}\right|^2 = \left|\frac{1}{1+\alpha}\right|^2 = \frac{1}{1+2C_\alpha\epsilon^\delta+C_\alpha^2\epsilon^{2\delta}}$$
$$= 1-2C_\alpha\epsilon^\delta+\mathcal{O}(\epsilon^{2\delta}),$$

which concludes the proof. □

Theorem 4 *For the OWR algorithm with no overlap, $n = 0$ and for small $\epsilon > 0$, if $\alpha_0^* = \sqrt{2}\epsilon^{1/4}$, then the convergence factor ρ_0 satisfies*

$$|\rho_0(\omega,\alpha)| \le |\rho_0(0,\alpha_0^*)| \sim 1-2\sqrt{2}\epsilon^{1/4}+\mathcal{O}(\epsilon^{1/2}). \tag{22}$$

Proof For the non-overlapping case, the solution of the min-max problem (17) is given by equi-oscillation for $\omega = 0$ and $\omega \to \infty$, see the left plot of Fig. 9. Lemma 5 provides us the expressions for $|\rho_0(0,\alpha)|$ and $|\rho_0(\infty,\alpha)|$ which are equal for α_0^*. Comparing the powers of the dominating terms of these expressions results in $\frac{1}{2}-\delta = \delta$ which implies $\delta = \frac{1}{4}$. Now, equating the coefficients of these dominating terms gives $C_\alpha = \sqrt{2}$ and this completes the proof. □

The analysis is different for the overlapping case $n > 0$. Numerically, we observe that the solution of the min-max problem (17) is also given by equi-oscillation, see the right plot of Fig. 9. But in this case, equi-oscillation for $|\rho_n(\omega,\alpha)|$ occurs for $\omega = 0$ and $\omega = \tilde{\omega}$, where $\tilde{\omega} \to 0$ as $\epsilon \to 0$. The dependence of the optimized α^* and $\tilde{\omega}$ on ϵ for $n = 1$ can be seen in the right plot of Figs. 10 and 11. We therefore use the ansatz $\tilde{\omega} := C_\omega\epsilon^\eta$, for some $\eta > 0$. Solving the problem (17) is equivalent to solving the system of equations

$$|\rho_n(0,\alpha_n^*)| = |\rho_n(\tilde{\omega},\alpha_n^*)| \quad \text{and} \quad \frac{\partial}{\partial\omega}|\rho(\tilde{\omega},\alpha_n^*)| = 0, \tag{23}$$

where α_n^* is the optimized α for an overlap of size n. We first solve the equation $\frac{\partial}{\partial\omega}|\rho(\tilde{\omega},\alpha_n^*)| = 0$ and find a relation between $\tilde{\omega}$ and α_n^*. Substituting this relation into the first equation of (23) then gives an explicit expression for α_n^*.

Lemma 6 *For the overlapping case, $n > 0$, solving $\frac{\partial}{\partial\omega}|\rho(\tilde{\omega},\alpha_n^*)| = 0$ gives us the relation*

$$\eta = \delta \quad \text{and} \quad C_\omega = \frac{2a}{n}C_\alpha, \tag{24}$$

where $\tilde{\omega} = C_\omega\epsilon^\eta$ and $\alpha_n^* = C_\alpha\epsilon^\delta$.

Proof We recall the expression for the convergence factor (13) for the OWR algorithm with n overlap,

$$|\rho_n(\omega,\alpha)| = \left|\left(\frac{\alpha+1-\lambda_1}{(1+\alpha)\lambda_1-1}\right)^2\left(\frac{1}{\lambda_1^2}\right)^n\right| = |\rho_0(\omega,\alpha)|\left|\left(\frac{1}{\lambda_1^2}\right)^n\right| = \frac{A(\omega,\alpha)}{B(\omega,\alpha)}D(\omega),$$

where $\lambda_1 = x + iy$ and

$$A(\omega,\alpha) = |\alpha+1-\lambda_1|^2 = \alpha^2+x^2+1+y^2-2x-2x\alpha+2\alpha,$$
$$B(\omega,\alpha) = |(1+\alpha)\lambda_1-1|^2 = y^2+1-2x+2\alpha y^2-2x\alpha+2\alpha x^2+x^2+y^2\alpha^2+x^2\alpha^2,$$
$$D(\omega) = \left|\left(\frac{1}{\lambda_1^2}\right)^n\right| = \left(\frac{1}{x^2+y^2}\right)^n.$$

We express $A(\omega,\alpha)$, $B(\omega,\alpha)$ and $D(\omega)$ as polynomials in ω and then find their derivative with respect to ω. In the proof of Lemma 4, we defined $x = \frac{(2+\epsilon)a+z_1}{2a}$ and $y = \frac{\omega+z_2}{2a}$, where $z_1 + iz_2 = \sqrt{r+ip}$ and hence

$$z_1^2 - z_2^2 = r \quad \text{and} \quad 2z_1z_2 = p.$$

Solving these two equations results in solving $z_2 = \frac{p}{2z_1}$ and $4z_1^4 - 4z_1^2r - p^2 = 0$, which gives $z_1^2 = \frac{r+\sqrt{r^2+p^2}}{2}$. Let $rs := \sqrt{r^2+p^2}$, where $r := \epsilon^2a^2 - \omega^2 + 4\epsilon a^2$ and $p := 2(2+\epsilon)\omega a$. A Taylor expansion for $(1+y)^{1/2}$, $y < 1$, leads for rs to

$$\begin{aligned} rs &= \sqrt{r^2+p^2} = \sqrt{(-\omega^2+4a^2\epsilon+a^2\epsilon^2)^2+4\omega^2a^2(2+\epsilon)^2} \\ &= \sqrt{16a^2\omega^2+\omega^4+8\omega^2a^2\epsilon+16\epsilon^2a^4+\dots} \\ &= 4\omega a\sqrt{1+\left(\frac{\omega^2}{16a^2}+\frac{\epsilon}{2}+\frac{a^2\epsilon^2}{\omega^2}+\dots\right)} \\ &= 4\omega a+\frac{\omega^3}{8a}+\omega a\epsilon+\frac{2a^3\epsilon^2}{\omega}+\mathcal{O}(\omega^5). \end{aligned}$$

Similarly, we obtain expressions for z_1 and z_2,

$$\begin{aligned} z_1 &= \sqrt{\frac{r+rs}{2}} \\ &= \sqrt{2a\omega}\sqrt{1-\frac{\omega}{4a}+\frac{\omega^2}{32a^2}+\frac{a\epsilon}{\omega}+\frac{\epsilon}{4}+\frac{a\epsilon^2}{4\omega}+\dots} \\ &= \sqrt{2a\omega}-\frac{\sqrt{2}\omega^{3/2}}{8\sqrt{a}}+\frac{\sqrt{2}\omega^{5/2}}{128a^{3/2}}+\frac{\sqrt{2}a^{3/2}\epsilon}{2\sqrt{\omega}}+\mathcal{O}(w^{1/2}\epsilon), \end{aligned}$$

and $z_2 = \frac{p}{2z_1} = \sqrt{2a\omega}+\frac{\sqrt{2}\omega^{3/2}}{8\sqrt{a}}-\frac{\sqrt{2}a^{3/2}\epsilon}{2\sqrt{\omega}}+\mathcal{O}(w^{1/2}\epsilon)$. Substituting these into the expressions for x and y leads to

$$x = 1+\frac{\sqrt{2}\sqrt{\omega}}{2\sqrt{a}}-\frac{\sqrt{2}\omega^{3/2}}{16a^{3/2}}+\mathcal{O}(\omega^{5/2}),$$
$$y = \frac{\sqrt{2}\sqrt{\omega}}{2\sqrt{a}}+\frac{\omega}{2a}+\frac{\sqrt{2}\omega^{3/2}}{16a^{3/2}}+\mathcal{O}(\omega^{5/2}).$$

Collecting the dominating terms gives us asymptotic expressions for $A(\omega,\alpha)$ and $B(\omega,\alpha)$,

$$A(\omega,\alpha) = \frac{\omega}{a} - \frac{\sqrt{2}C_\alpha\epsilon^\delta\sqrt{\omega}}{\sqrt{a}} + \frac{\sqrt{2}\omega^{3/2}}{2a^{3/2}} + \mathcal{O}(\omega^2),$$
$$B(\omega,\alpha) = \frac{\omega}{a} + \frac{\sqrt{2}C_\alpha\epsilon^\delta\sqrt{\omega}}{\sqrt{a}} + \frac{\sqrt{2}\omega^{3/2}}{2a^{3/2}} + \mathcal{O}(\omega^2).$$

To find an asymptotic expression for $D(\omega)$, we use the Taylor expansion $\left(\frac{1}{1+y}\right)^n = 1 - ny + \frac{n^2y^2}{2} + \mathcal{O}(y^3)$ and obtain

$$D(\omega) = \left(\frac{1}{x^2+y^2}\right)^n = \left(\frac{1}{1+\frac{\sqrt{2}\sqrt{\omega}}{\sqrt{a}} + \frac{\omega}{a} + \frac{3\sqrt{2}\omega^{3/2}}{8a^{3/2}} + \mathcal{O}(\omega^2)}\right)^n$$
$$= 1 - \frac{n\sqrt{2}\sqrt{\omega}}{\sqrt{a}} - \frac{n\omega}{a} + \frac{n^2\omega}{a} + \mathcal{O}(\omega^{3/2}). \tag{25}$$

Further, differentiating $|\rho_n(\omega,\alpha)| = \frac{A(\omega,\alpha)}{B(\omega,\alpha)}D(\omega)$ with respect to ω produces

$$\frac{\partial}{\partial\omega}|\rho_n(\omega,\alpha)| = \frac{B(\omega,\alpha)[A(\omega,\alpha)D_\omega(\omega) + A_\omega(\omega,\alpha)D(\omega)] - A(\omega,\alpha)D(\omega)B_\omega(\omega,\alpha)}{B^2(\omega,\alpha)}.$$

Let $F_1(\omega,\alpha) := B(\omega,\alpha)[A(\omega,\alpha)D_\omega(\omega) + A_\omega(\omega,\alpha)D(\omega)]$ and $F_2(\omega,\alpha) := A(\omega,\alpha)D(\omega)$ $B_\omega(\omega,\alpha)$, where $A_\omega(\omega,\alpha)$ denotes the partial derivative of $A(\omega,\alpha)$ with respect to ω. Collecting the dominating terms in the asymptotic expansions of F_1, F_2 results in

$$F_1(\omega,\alpha) = \frac{\sqrt{2}C_\alpha\epsilon^\delta\sqrt{\omega}}{2a^{3/2}} + \frac{\omega}{a^2} + \frac{\sqrt{2}\omega^{3/2}}{2a^{5/2}}\left(\frac{5}{2} - 3n\right) + \mathcal{O}(\omega^2),$$
$$F_2(\omega,\alpha) = -\frac{\sqrt{2}C_\alpha\epsilon^\delta\sqrt{\omega}}{2a^{3/2}} + \frac{\omega}{a^2} + \frac{\sqrt{2}\omega^{3/2}}{a^{5/2}}\left(\frac{5}{4} - n\right) + \mathcal{O}(\omega^2).$$

Equating $F_1(\tilde{\omega},\alpha) - F_2(\tilde{\omega},\alpha) = 0$, we obtain $\tilde{\omega} = \frac{2aC_\alpha}{n}\epsilon^\delta$. Since we use the ansatz $\tilde{\omega} = C_\omega\epsilon^\eta$, comparing the exponents and coefficients simplifies to (24) and this completes the proof. □

Now we need to solve the first equation of (23), $|\rho_n(0,\alpha_n^*)| = |\rho_n(\tilde{\omega},\alpha_n^*)|$. We do this in a similar way as for the non-overlapping case, $n = 0$. We express $|\rho_n(0,\alpha_n^*)|$ and $|\rho_n\tilde{\omega},\alpha_n^*)|$ as asymptotic expansions in ϵ.

Lemma 7 *For the overlapping case, $n > 0$, the modulus of the convergence factor $|\rho_n(\omega,\alpha)|$ for the OWR algorithm for $\omega = 0$ and $\omega = \tilde{\omega}$ is for small ϵ given by*

$$|\rho_n(0,\alpha)| = 1 - \frac{4}{C_\alpha}\epsilon^{\frac{1}{2}-\delta} + \mathcal{O}(\epsilon^{1-2\delta}), \tag{26}$$

and

$$|\rho_n(\tilde{\omega},\alpha)| = 1 - \frac{2\sqrt{2}C_\alpha\sqrt{a}\epsilon^{\delta/2}}{\sqrt{C_\omega}} - \frac{n\sqrt{2}\sqrt{C_\omega}\epsilon^{\delta/2}}{\sqrt{a}} + \mathcal{O}(\epsilon^\delta). \tag{27}$$

Proof From the polynomial expansion of $D(\omega)$ given in (25), we obtain $D(0) = \left|\left(\frac{1}{\lambda_1^2(0)}\right)^n\right| = 1$. Substituting this into the formula for the convergence factor for OWR

with n overlap leads to $|\rho_n(0,\alpha)| = |\rho_0(0,\alpha)|\left|\left(\frac{1}{\lambda_1^2(0)}\right)^n\right| = |\rho_0(0,\alpha)|$ and we arrive at (26).

The analysis to find the expression for $|\rho_n(\tilde{\omega},\alpha)|$ is similar. Substituting $\tilde{\omega} = C_\omega\epsilon^\delta$ in to the expressions for $A(\omega,\alpha)$ and $B(\omega,\alpha)$ leads to

$$\begin{aligned}
A(\tilde{\omega},\alpha) &= \frac{\tilde{\omega}}{a} - \frac{\sqrt{2}C_\alpha\epsilon^\delta\sqrt{\tilde{\omega}}}{\sqrt{a}} + \frac{\sqrt{2}\tilde{\omega}^{3/2}}{2a^{3/2}} + \mathcal{O}(\tilde{\omega}^2) = \frac{C_\omega\epsilon^\delta}{a} - \frac{\sqrt{2}C_\alpha\sqrt{C_\omega}\epsilon^{3\delta/2}}{\sqrt{a}} \\
&\quad + \frac{C_\omega^{3/2}\epsilon^{3\delta/2}}{\sqrt{2}a^{3/2}} + \mathcal{O}(\epsilon^{2\delta}) \\
&= \frac{C_\omega\epsilon^\delta}{a}\left(1 - \frac{\sqrt{2}C_\alpha\sqrt{a}\epsilon^{\delta/2}}{\sqrt{C_\omega}} + \frac{\sqrt{C_\omega}\epsilon^{\delta/2}}{\sqrt{2}\sqrt{a}} + \mathcal{O}(\epsilon^\delta)\right), \\
B(\tilde{\omega},\alpha) &= \frac{\tilde{\omega}}{a} + \frac{\sqrt{2}C_\alpha\epsilon^\delta\sqrt{\tilde{\omega}}}{\sqrt{a}} + \frac{\sqrt{2}\tilde{\omega}^{3/2}}{2a^{3/2}} + \mathcal{O}(\tilde{\omega}^2) = \frac{C_\omega\epsilon^\delta}{a} + \frac{\sqrt{2}C_\alpha\sqrt{C_\omega}\epsilon^{3\delta/2}}{\sqrt{a}} \\
&\quad + \frac{C_\omega^{3/2}\epsilon^{3\delta/2}}{\sqrt{2}a^{3/2}} + \mathcal{O}(\epsilon^{5\delta/2}) \\
&= \frac{C_\omega\epsilon^\delta}{a}\left(1 + \frac{\sqrt{2}C_\alpha\sqrt{a}\epsilon^{\delta/2}}{\sqrt{C_\omega}} + \frac{\sqrt{C_\omega}\epsilon^{\delta/2}}{\sqrt{2}\sqrt{a}} + \mathcal{O}(\epsilon^\delta)\right).
\end{aligned}$$

Dividing $A(\tilde{\omega},\alpha)$ by $B(\tilde{\omega},\alpha)$ and using the Taylor expansion $\frac{1}{1+z} = 1 - z + \frac{z^2}{2} + \mathcal{O}(z^3)$ gives us

$$\begin{aligned}
\frac{A(\tilde{\omega},\alpha)}{B(\tilde{\omega},\alpha)} &= \left(1 - \frac{\sqrt{2}C_\alpha\sqrt{a}\epsilon^{\delta/2}}{\sqrt{C_\omega}} + \frac{\sqrt{C_\omega}\epsilon^{\delta/2}}{\sqrt{2}\sqrt{a}} + \ldots\right)\left(1 - \frac{\sqrt{2}C_\alpha\sqrt{a}\epsilon^{\delta/2}}{\sqrt{C_\omega}} - \frac{\sqrt{C_\omega}\epsilon^{\delta/2}}{\sqrt{2}\sqrt{a}} + \ldots\right) \\
&= 1 - \frac{2\sqrt{2}C_\alpha\sqrt{a}\epsilon^{\delta/2}}{\sqrt{C_\omega}} - \frac{C_\omega\epsilon^\delta}{2a} + \frac{2C_\alpha^2 a\epsilon^\delta}{C_\omega} + \mathcal{O}(\epsilon^{3\delta/2}).
\end{aligned}$$

Similarly, we obtain the expression for $D(\tilde{\omega})$,

$$D(\tilde{\omega}) = 1 - \frac{n\sqrt{2}\sqrt{C_\omega}\epsilon^{\delta/2}}{\sqrt{a}} - \frac{nC_\omega\epsilon^\delta}{a} + \frac{n^2C_\omega\epsilon^\delta}{a} + \mathcal{O}(\epsilon^{3\delta/2}).$$

Multiplying the above expression by the expansion for $\frac{A(\tilde{\omega})}{B(\tilde{\omega})}$, we find,

$$\begin{aligned}
|\rho_n(\tilde{\omega},\alpha)| &= \left(1 - \frac{2\sqrt{2}C_\alpha\sqrt{a}\epsilon^{\delta/2}}{\sqrt{C_\omega}} - \frac{C_\omega\epsilon^\delta}{2a} + \frac{2C_\alpha^2 a\epsilon^\delta}{C_\omega} + \mathcal{O}(\epsilon^{3\delta/2})\right) \\
&\quad \left(1 - \frac{n\sqrt{2}\sqrt{C_\omega}\epsilon^{\delta/2}}{\sqrt{a}} - \frac{nC_\omega\epsilon^\delta}{a} + \mathcal{O}(\epsilon^{3\delta/2})\right) \\
&= 1 - \frac{2\sqrt{2}C_\alpha\sqrt{a}\epsilon^{\delta/2}}{\sqrt{C_\omega}} - \frac{n\sqrt{2}\sqrt{C_\omega}\epsilon^{\delta/2}}{\sqrt{a}} + \mathcal{O}(\epsilon^\delta),
\end{aligned}$$

which completes the proof. □

We are now ready to prove a remarkably simple formula for the optimized parameter depending on the overlap $n > 0$ which is quite different from the non-overlapping case:

Theorem 5 *For the OWR algorithm in the overlapping case, $n > 0$, and for small $\epsilon > 0$, if $\alpha_n^* = \left(\frac{\epsilon}{n}\right)^{1/3}$, then the convergence factor ρ_n satisfies*

$$|\rho_n(\omega, \alpha)| \leq |\rho_n(0, \alpha_n^*)| \sim 1 - 4n^{1/3}\epsilon^{1/6} + \mathcal{O}(\epsilon^{1/3}). \tag{28}$$

Proof Since the solution of our min-max problem (17) is obtained numerically by equi-oscillation for $\omega = 0$ and $\omega = \tilde{\omega}$, equating the expansions for $|\rho_n(0, \alpha)|$ and $|\rho_n(\tilde{\omega}, \alpha)|$ given by (26) and (27) and comparing their dominating terms, we obtain

$$\frac{\delta}{2} = \frac{1}{2} - \delta \quad \text{and} \quad \frac{4}{C_\alpha} = \frac{2\sqrt{2}C_\alpha\sqrt{a}}{\sqrt{C_\omega}} + \frac{n\sqrt{2}\sqrt{C_\omega}}{\sqrt{a}}.$$

The first equation implies that $\delta = 1/3$, and substituting the expression for C_ω given by (24) results in $C_\alpha = \left(\frac{1}{n}\right)^{1/3}$. This completes the proof of the theorem. □

6 Multiple Sub-circuits

We studied so far only the decomposition of the system of Eq. (1) into two sub-systems. However, for the practical use on parallel computers, we need to split the system into many sub-systems and apply the WR or OWR algorithm to them. We thus split the RC circuit of infinite length in Fig. 1 into N_s sub-circuits which are denoted by $\mathbf{v}_r$, $r = 1, 2, \ldots, N_s$. Assume that each sub-circuit $\mathbf{v}_r$ contains M_r nodes. Applying the optimized waveform relaxation algorithm (with α, β as the optimization parameters) with n nodes overlap leads to

$$\begin{aligned}
\dot{\mathbf{v}}_1^{k+1}(t) &= \begin{bmatrix} \ddots & \ddots & \ddots & \\ & a & b & a \\ & & a & b + \frac{a}{\alpha+1} \end{bmatrix} \mathbf{v}_1^{k+1}(t) + \begin{bmatrix} \vdots \\ 0 \\ a v_{2,n+1}^k(t) - \frac{a}{\alpha+1} v_{2,n}^k(t) \end{bmatrix}, \\
\dot{\mathbf{v}}_r^{k+1}(t) &= \begin{bmatrix} b - \frac{a}{\beta-1} & a & & \\ a & b & a & \\ & \ddots & \ddots & \ddots \\ & & a & b + \frac{a}{\alpha+1} \end{bmatrix} \mathbf{v}_r^{k+1}(t) + \begin{bmatrix} a v_{r-1,M_r}^k(t) + \frac{a}{\beta-1} v_{r-1,M_r+1}^k(t) \\ 0 \\ \vdots \\ 0 \\ a v_{r+1,n+1}^k(t) - \frac{a}{\alpha+1} v_{r+1,n}^k(t) \end{bmatrix}, \\
\dot{\mathbf{v}}_{N_s}^{k+1}(t) &= \begin{bmatrix} b - \frac{a}{\beta-1} & a & & \\ a & b & a & \\ & \ddots & \ddots & \ddots \end{bmatrix} \mathbf{v}_{N_s}^{k+1}(t) + \begin{bmatrix} a v_{N_s-1,M_r}^k(t) + \frac{a}{\beta-1} v_{N_s-1,M_r+1}^k(t) \\ 0 \\ \vdots \end{bmatrix},
\end{aligned} \tag{29}$$

where $r = 2, 3, \ldots, N_s - 1$ and we have considered the source term $\mathbf{f} = 0$ for simplicity. For $\alpha = \infty$, $\beta = -\infty$, we obtain the classical Waveform Relaxation algorithm.

In the case of OWR for two sub-domains, we saw that with the optimal transmission conditions (15), convergence is achieved in 2 iterations and the parameters α, β represent non-local operators in time. In the case of N_s sub-circuits, with the use of optimal transmission conditions, one can show that convergence can be achieved in N_s iterations [16], and this result still holds in the overlapping case. Again these parameters α, β are non-local operators in time and the analysis becomes very complicated.[1] Hence we will use α_0^* and α_n^* given

[1] For an early approximate numerical optimization, see [8], which followed a presentation of the first author at SciCADE 99 on why WR methods are slow, and a followup discussion. At the PDE level this problem is in the meantime much better understood, see [18] for a review.

Theorems 4 and 5 from our two sub-circuit analysis and test their performance numerically for the multiple sub-circuit case.

7 Numerical Results

We consider an RC circuit with $R = 0.5k\Omega$, $C = 0.63pF$, $a = \frac{1}{RC}$ and $b = -(2+\epsilon)a$ with $\epsilon > 0$, $\epsilon \to 0$, and we always specify the time T in nano-seconds (ns). Our analysis for both WR and OWR was performed assuming that the length of the circuit is infinite. For our numerical experiments, we consider a circuit of length $N = 200$, a homogeneous source, zero initial conditions, and apply the backward Euler scheme for time integration with $\Delta t = 0.1$ and $T = 2000$. We use random initial guesses to start both the WR and OWR algorithm. The left plot of Fig. 12 clearly shows the important influence of our optimized transmission conditions (10) on the convergence of the algorithm. We used the optimized α for OWR given in Theorems 4 and 5. We also illustrate in the same figure the influence of overlap on convergence. Increasing the overlap increases the convergence rate in both the WR and OWR algorithm, but the impact of the optimized transmission conditions is much more important for performance than the influence of the overlap.

We have seen in (2) that for $\epsilon \to 0$, the RC circuit of infinite length is an approximation to the one dimensional heat equation. We now apply the WR and OWR algorithms with different overlaps $n = 0$ and $n = 2$ to the heat equation (2). For OWR we need the values of α_0^* and α_2^*, which we obtain both by solving the min-max problem numerically, and by using the asymptotic expression in Theorems 4 and 5 respectively from our circuit analysis for small $\epsilon = 10^{-4}$. From the right plot of Fig. 12, we observe that OWR converges much faster than WR. Also, the numerically calculated α_0^* and α_2^* give us the best convergence. For overlap $n = 2$, the convergence of OWR using our asymptotic expression for α_2^* for $\epsilon = 10^{-4}$ needs only 4 more iterations, than the best possible choice computed numerically. This is very little compared to the iterations and time required to compute α_2^* numerically. This shows that our expressions in Theorems 4 and 5 can also be used when OWR is applied to the heat equation.

We next compare the numerically and asymptotically optimized values of α_n^*. For the non-overlapping case $n = 0$ and $\epsilon = 10^{-4}$, we show in Fig. 13 on the left the error reduction for different values of α, together with the numerically and asymptotically optimized value. We see that our asymptotic formula underestimates the optimal choice a bit. However, the right

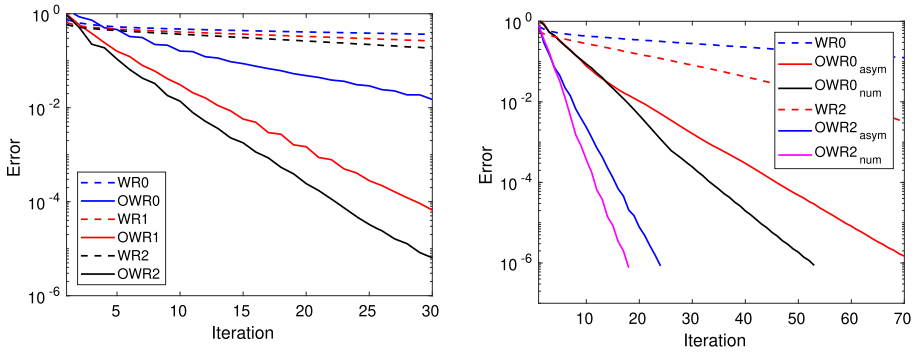

Fig. 12 Convergence for $T = 2000$ for the RC circuit (left) and for the heat equation (right)

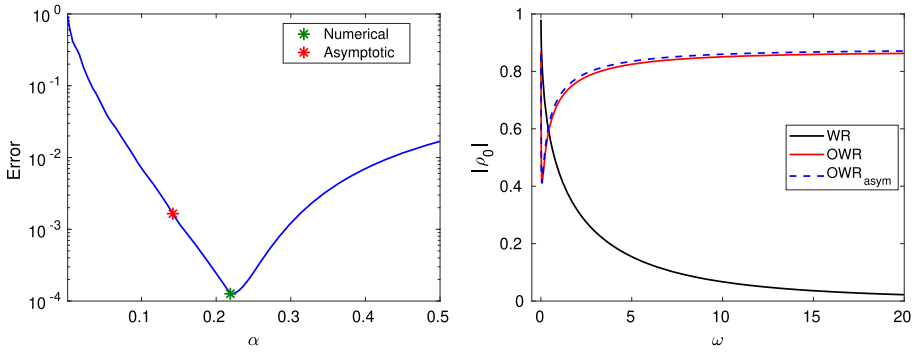

Fig. 13 Comparison of the optimized α for $\epsilon = 10^{-4}$ for $n = 0$ (left) and convergence factor for $n = 0$ in Laplace space for WR and OWR (right)

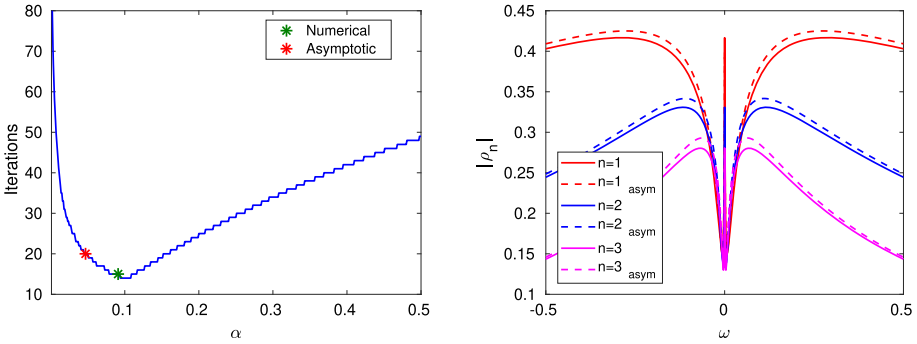

Fig. 14 Comparison of the optimized α for $\epsilon = 10^{-4}$ for $n = 1$ (left) and comparison of the convergence factor for different overlaps for OWR (right)

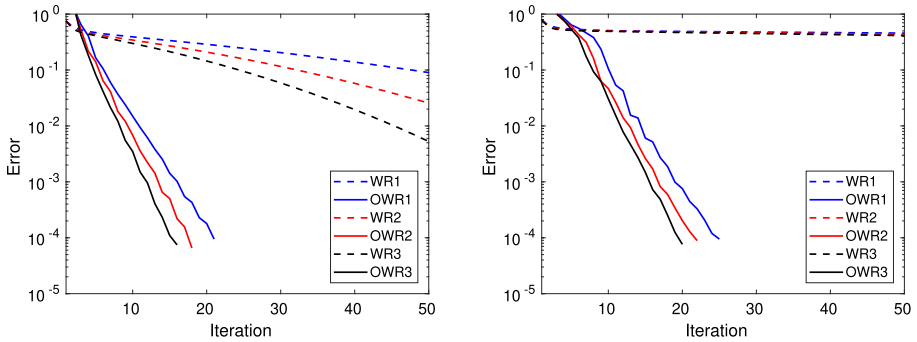

Fig. 15 Convergence for $T = 1000$ for multiple sub-circuits $N_s = 5$ (left) and for $N_s = 50$ (right)

plot in Fig. 13 shows that for the two different values of the optimized α, the corresponding convergence factors $|\rho_0|$ in Laplace space are very close to each other, and we also show the improvement in the overall convergence for OWR compared to WR. In Fig. 14 we show the corresponding results for the overlapping case $n > 0$, and the observations are similar as for $n = 0$.

Finally, we consider the case when we split our RC circuit with size $N = 1000$ into multiple sub-circuits. We choose $\epsilon = 10^{-5}$ and $T = 1000$, with zero initial condition, homogeneous source and random initial guesses. We use our optimized α in in Theorem 5 from the two sub-circuit analysis. We first consider $N_s = 5$ and then $N_s = 50$ sub-circuits. We see in Fig. 15 that our asymptotically optimized parameters for two sub-circuits work extremely well for the many sub-circuit case, and make the OWR solver into a rather effective method for solving many sub-circuit problems.

8 Conclusion

We presented a first analysis for the influence of overlap on the convergence factor for both the WR and OWR methods applied to RC circuits. We found that increasing the overlap increases the convergence rate for both WR and OWR, but the impact of optimized transmission conditions is far more important than the impact of overlap. The overlap however changes the optimized parameters, and we provided closed form asymptotic formulas for them. Using OWR with these parameters leads to much lower iteration counts, also when OWR is used for many sub-circuits. We also showed that our optimized parameters can be used when solving heat equations with waveform relaxation techniques. A final important contribution is our interpretation of these optimized transmission conditions as circuit elements, which should help circuit designers to better understand and embrace this new technology.

Funding Funding was provided by Schweizerischer Nationalfonds zur Förderung der Wissenschaftlichen Forschung (Grant No. 200020_168999 and 200020_178752).

References

1. Al-Khaleel, M., Gander, M.J., Ruehli, A.E.: Optimized waveform relaxation solution of RLCG transmission line type circuits. In: 9th International Conference on Innovations in Information Technology (IIT), pp 136–140 (2013)
2. Al-Khaleel, M., Gander, M.J., Ruehli, A.E.: A mathematical analysis of optimized waveform relaxation for a small RC circuit. In: 10th IMACS International Symposium on Iterative Methods in Scientific Computing, Applied Numerical Mathematics vol. 75, pp. 61–76 (2014)
3. Al-Khaleel, M., Gander, M.J., Ruehli, A.E.: Optimization of transmission conditions in waveform relaxation techniques for RC circuits. SIAM J. Numer. Anal. **52**, 1076–1101 (2014)
4. Bortot, L., Auchmann, B., Garcia, I.C., Navarro, A.M.F., Maciejewski, M., Mentink, M., Prioli, M., Ravaioli, E., Schöps, S., Verweij, A.P.: STEAM: a hierarchical cosimulation framework for superconducting accelerator magnet circuits. IEEE Trans. Appl. Supercond. **28**(3), 1–6 (2018). https://doi.org/10.1109/TASC.2017.2787665
5. Brenner, S., Scott, R.: The Mathematical Theory of Finite Element Methods. Texts in Applied Mathematics. Springer, New York (2007)
6. Burrage, K.: Parallel and Sequential Methods for Ordinary Differential Equations. Clarendon Press, Oxford (1995)
7. Burrage, K., Jackiewicz, Z., Nørsett, S., Renaut, R.A.: Preconditioning waveform relaxation iterations for differential systems. BIT Numer. Math. **36**, 54–76 (1996)
8. Burrage, K., Hertono, G., Jackiewicz, Z., Welfert, B.D.: Acceleration of convergence of static and dynamic iterations. BIT Numer. Math. **41**, 645–655 (2001)
9. Burrage, K., Jackiewicz, Z., Welfert, B.: Spectral approximation of time windows in the solution of dissipative linear differential equations. J. Numer. Anal. Ind. Appl. Math. **4**(1–2), 41–64 (2009)
10. Christlieb, A.J., Macdonald, C.B., Ong, B.W.: Parallel high-order integrators. SIAM J Sci. Comput. **32**, 818–835 (2010)

11. de Dieu Nshimiyimana, J., Plumier, F., Dular, P., Geuzaine, C., Gyselinck, J.: Co-simulation of finite element and circuit solvers using optimized waveform relaxation. In: IEEE International Energy Conference (ENERGYCON), pp. 1–6(2016). https://doi.org/10.1109/ENERGYCON.2016.7513958
12. Dolean, V., Jolivet, P., Nataf, F.: An introduction to domain decomposition methods. In: Algorithms, Theory, and Parallel Implementation . Society for Industrial and Applied Mathematics (SIAM), Philadelphia, PA (2015)
13. Gander, M.J., Halpern, L.: Méthodes de relaxation d'ondes (SWR) pour l'èquation de la chaleur en dimension 1. C. R. Math. **336**(6), 519–524 (2003)
14. Gander, M.J., Kwok, F.: Numerical Analysis of Partial Differential Equations Using Maple and MATLAB. Society for Industrial and Applied Mathematics, Philadelphia (2018). https://doi.org/10.1137/1.9781611975314
15. Gander, M.J., Ruehli, A.E.: Solution of large transmission line type circuits using a new optimized waveform relaxation partitioning. In: IEEE Symposium on Electromagnetic Compatibility. Symposium Record (Cat. No.03CH37446), vol. 2, pp. 636–641 (2003)
16. Gander, M.J., Ruehli, A.E.: Optimized waveform relaxation methods for RC type circuits. IEEE Trans. Circuits Syst. I Regul. Pap. **51**(4), 755–768 (2004)
17. Gander, M.J., Stuart, A.: Space–time continuous analysis of waveform relaxation for the heat equation. SIAM J. Sci. Comput. **19**(6), 2014–2031 (1998)
18. Gander, M.J., Zhang, H.: A class of iterative solvers for the helmholtz equation: factorizations, sweeping preconditioners, source transfer, single layer potentials, polarized traces, and optimized Schwarz methods. SIAM Rev. **61**(1), 3–76 (2019)
19. Gander, M.J., Halpern, L., Nataf, F.: Optimal Schwarz waveform relaxation for the one dimensional wave equation. SIAM J. Numer. Anal. **41**(5), 1643–1681 (2003)
20. Gander, M.J., Al-Khaleel, M., Ruehli, A.E.: Waveform relaxation technique for longitudinal partitioning of transmission lines. In: IEEE Electrical Performance of Electronic Packaging, pp. 207–210 (2006)
21. Gander, M.J., Al-Khaleel, M., Ruchli, A.E.: Optimized waveform relaxation methods for longitudinal partitioning of transmission lines. IEEE Trans. Circuits Syst. I Regul. Pap. **56**(8), 1732–1743 (2009)
22. Gander, M.J., Jiang, Y.L., Li, R.J.: Parareal Schwarz waveform relaxation methods. In: Bank, R., Holst, M., Widlund, O., Xu, J. (eds.) Domain Decomposition Methods in Science and Engineering, XX, pp. 451–458. Springer, Berlin (2013)
23. Gander, M.J., Kumbhar, P.M., Ruehli, A.E.: Analysis of overlap in waveform relaxation methods for RC circuits. In: Bjørstad, P.E., Brenner, S.C., Halpern, L., Kim, H.H., Kornhuber, R., Rahman, T., Widlund, O.B. (eds.) Domain Decomposition Methods in Science and Engineering XXIV, pp. 281–289. Springer International Publishing, Cham (2018)
24. Gander, M.J., Jiang, Y.L., Song, B.: A superlinear convergence estimate for the parareal Schwarz waveform relaxation algorithm. SIAM J. Sci. Comput. **41**(2), A1148–A1169 (2019)
25. Gander, M.J., Kumbhar, P.M., Ruehli, A.E.: Asymptotic analysis for different partitionings of RLC transmission lines. In: Accepted for Domain Decomposition Methods in Science and Engineering XXV, LNCSE, Springer, Berlin (2019)
26. Garcia, I.C., Schöps, S., Maciejewski, M., Bortot, L., Prioli, M., Auchmann, B., Verweij, A.: Optimized field/circuit coupling for the simulation of quenches in superconducting magnets. IEEE J. Multiscale Multiphys. Comput. Tech. **2**, 97–104 (2017). https://doi.org/10.1109/JMMCT.2017.2710128
27. Gaspar, F.J., Rodrigo, C.: Multigrid waveform relaxation for the time-fractional heat equation. SIAM J. Sci. Comput. **39**(4), A1201–A1224 (2017)
28. Griffiths, D.F.: Finite Element Methods for Time Dependent Problems, pp. 327–357. Springer, Dordrecht (1986)
29. Ho, C.W., Ruehli, A., Brennan, P.: The modified nodal approach to network analysis. IEEE Trans. Circuits Syst. **22**(6), 504–509 (1975)
30. Janssen, J., Vandewalle, S.: Multigrid waveform relaxation of spatial finite element meshes: the continuous-time case. SIAM J. Numer. Anal. **33**(2), 456–474 (1996a)
31. Janssen, J., Vandewalle, S.: Multigrid waveform relaxation on spatial finite element meshes: the discrete-time case. SIAM J. Sci. Comput. **17**(1), 133–155 (1996b)
32. Jeltsch, R., Pohl, B.: Waveform relaxation with overlapping splittings. SIAM J. Sci. Comput. **16**(1), 40–49 (1995)
33. Kumbhar, P.M.: Asymptotic analysis of optimized waveform relaxation methods for RC circuits and RLCG transmission lines. PhD thesis, iD: unige:136729 (2020)
34. Kwok, F., Ong, B.: Schwarz waveform relaxation with adaptive pipelining. SIAM J. Sci. Comput. **41**(1), A339–A364 (2019)

35. Lelarasmee, E., Ruehli, A.E., Sangiovanni-Vincentelli, A.L.: The waveform relaxation method for time-domain analysis of large scale integrated circuits. IEEE Trans. Comput. Aided Des. Integr. Circuits Syst. **1**(3), 131–145 (1982)
36. Menkad, T., Dounavis, A.: Resistive coupling-based waveform relaxation algorithm for analysis of interconnect circuits. IEEE Trans. Circuits Syst. I Regul. Pap. **64**(7), 1877–1890 (2017)
37. Najm, F.N.: Circuit Simulation. Wiley-IEEE Press, Amsterdam (2010)
38. Ong, B.W., Haynes, R.D., Ladd, K.: Algorithm 965: Ridc methods: a family of parallel time integrators. ACM Trans. Math. Softw. **43**(1), 8:1–8:13 (2016a). https://doi.org/10.1145/2964377
39. Ong, B.W., High, S., Kwok, F.: Pipeline Schwarz waveform relaxation. In: Dickopf, T., Gander, M.J., Halpern, L., Krause, R., Pavarino, L.F. (eds.) Domain Decomposition Methods in Science and Engineering XXII, pp. 363–370. Springer, Cham (2016b)
40. Ruehli, A.E., Zukowski, C.A.: Convergence of waveform relaxation for RC circuits. In: Coughran, W.M., Cole, J., Llyod, P., White, J.K. (eds.) Semiconductors, pp. 141–146. Springer, New York, New York (1994)
41. Sand, J., Burrage, K.: A Jacobi waveform relaxation method for ODEs. SIAM J. Sci. Comput. **20**(2), 534–552 (1998). https://doi.org/10.1137/S1064827596306562
42. Vandewalle, S.: Parallel Multigrid Waveform Relaxation for Parabolic Problems. Teubner-Verlag, Sonnewalde (1993)
43. Vandewalle, S., Piessens, R.: Multigrid Waveform Relaxation for Solving Parabolic Partial Differential Equations, pp. 377–388. Birkhäuser Basel, Basel (1991)
44. White, J.K., Sangiovanni-Vincentelli, A.L.: Relaxation Techniques for the Simulation of VLSI Circuits. Kluwer, Boston (1987)
45. Wu, S.-L., Al-Khaleel, M.D.: Optimized waveform relaxation methods for RC circuits: discrete case. ESAIM: M2AN **51**(1), 209–223 (2017)